SAND2012-2921P

Preliminary UV Propagation Modeling

Derek P. Young
Sandia National Laboratories
Livermore, CA 94551

January 24, 2011

Contents

1 Introduction

Communication using mid-ultraviolet radiation between 200 nm and 280 nm has received renewed attention due to advancements in UV LED emitters and unique propagation characteristics at these wavelengths [1, 2, 3]. Atmospheric gases absorb light at mid-UV so that receivers or sensors operating on the earth's surface receive no interference from solar radiation. This so-called "solar-blind" region of the spectrum allows the use of single-photon detection techniques. Also, UV light is strongly scattered by molecules in the air, enabling non-line-of-sight (NLOS) communication.

1.1 Optical Properties

The two optical properties that we consider are absorption and scattering. The discussion is limited to elastically scattered light—fluorescence and Raman scattering are not considered. Particles much smaller than the wavelength of light (this includes molecules in the air), can be described accurately by Rayleigh's theory of molecular scattering. Geometric optics are used to analyze very large particles. When particle diameter and wavelength are on the same order of magnitude, however, Mie scattering theory must be used [4].

Many of the equations for absorption and scattering involve the use of the dimensionless *size parameter* which is given by

$$\alpha = \frac{\pi d}{\lambda} \tag{1}$$

where d is the particle diameter, and λ is the wavelength of the incident light. As light travels along an axis, the intensity diminishes according to the Lambert-Beer law.

$$\frac{I}{I_0} = \exp(-k_e L) \tag{2}$$

This relationship shows that an light intensity decreases exponentially with path length, L. The extinction coefficient, k_e incorporates the effects of both

scattering and absorption:

$$k_e = k_s + k_a, \tag{3}$$

where k_s is the scattering coefficient and k_a is the absorption coefficient.

The *extinction efficiency*, Q_e, gives the ratio of power scattered and absorbed over incident power. It is related to the extinction coefficient by Equation 4, where N is the concentration of a monodisperse aerosol in particles per unit volume.

$$Q_e = \frac{4k_e}{\pi N d^2} \tag{4}$$

The extinction coefficients and efficiencies are a function of the wavelength of light and particle properties. The absolute index of refraction, m, characterizes the particle material, and the size parameter characterizes the particle size and wavelength. The index of refraction is complex for absorbing materials. Figure 1 plots the extinction efficiency of water as a function of size parameter. Interestingly, Q_e converges to 2 for large α.

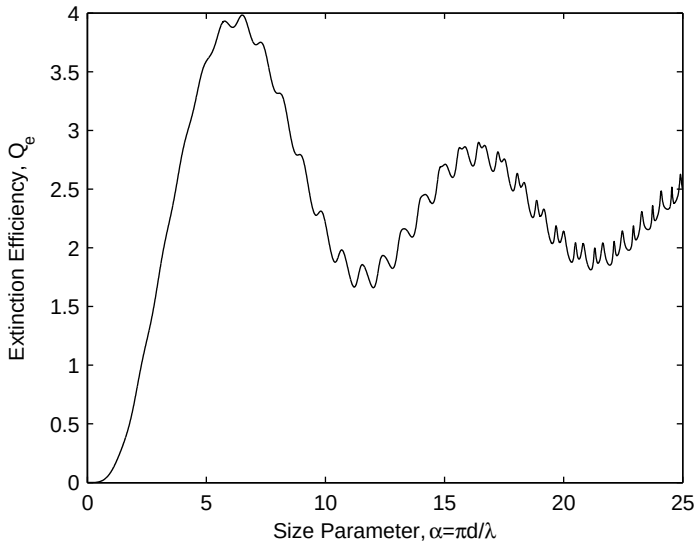

Figure 1: Extinction efficiency for water, m=1.33

Besides for extinction, the other phenomena of interest when considering UV propagation is angular scattering. When incident light hits a particle, light scatters as a function of angle as shown in Figure 2.

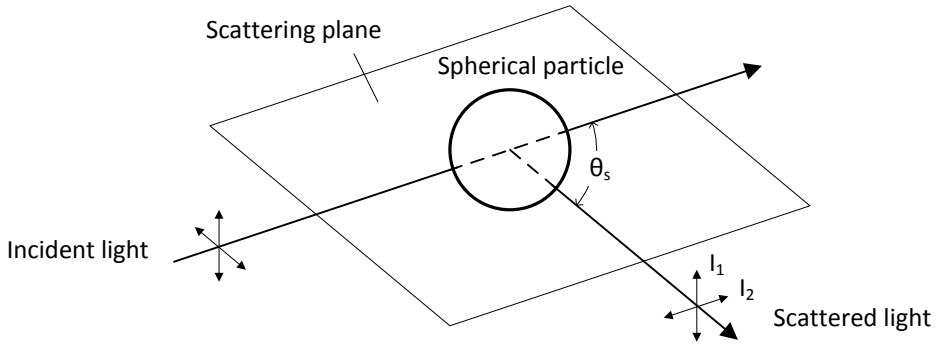

Figure 2: Diagram of scattering plane, scattering angle, and polarization components of scattered light [4]

For particles and molecules much smaller than the wavelength of incident light, the pattern and intensity is known as Rayleigh scattering. For an unpolarized source, the total intensity (in $\mathrm{W/m^2}$) at a distance R from the particle is given by

$$I(\theta_s) = \frac{I_0 \pi^4 d^6}{8R^2\lambda^4} \left(\frac{m^2-1}{m^2+2}\right)^2 (1+\cos^2\,\theta_s). \tag{5}$$

The *phase function* is a dimensionless and normalized version of the scattering function such that the integral of the phase function over 4π steradians equals 4π [5]. The phase function for total Rayleigh scattering is given by Equation 6. The phase function and its polarized components are plotted in Figure 3.

$$P(\theta_s) = \frac{3}{4}\left(1+\cos^2\,\theta_s\right). \tag{6}$$

The equations for Mie scattering are much more complex. The Mie scattering intensity is given by Equation 7, where i_1 and i_2 are the Mie intensity parameters for perpendicular and parallel polarizations, respectively. The

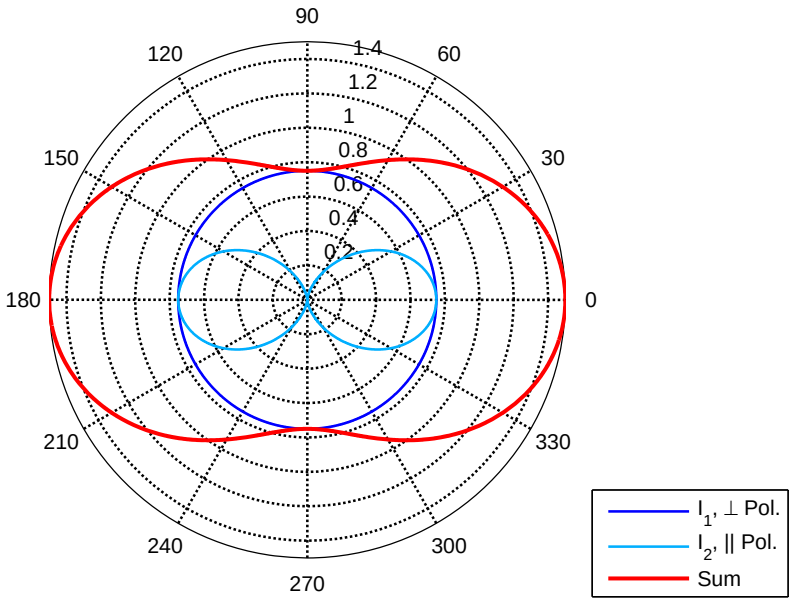

Figure 3: Rayleigh phase function

intensity parameters are functions of m, α, and θ_s. They are defined by an infinite series involve Legendre polynomials and Bessel functions [4].

$$I(\theta_s) = \frac{I_0 \lambda^2 (i_1 + i_2)}{8\pi^2 R^2} \tag{7}$$

To calculate the intensity parameters (as well as the extinction coefficients), we used publicly available MATLAB code written by Christian Mätzler, from the Institute of Applied Physics in Germany [6]. In order to find the phase function, intensity parameters produced by the code are integrated numerically. The normalized phase function for Mie scattering is then given by

$$P(\theta_s) = F(i_1 + i_2), \tag{8}$$

where F is the normalization factor. This factor is computed by integrating i_1 and i_2 over the surface of a sphere and taking the inverse, as shown in

Equation 9. The dependence of i_1 and i_2 on ϕ is explicitly shown.

$$F = 4\pi \left[2\pi \int_0^{\pi} [i_1(\phi) + i_2(\phi)] \sin\, \phi \, \mathrm{d}\phi \right]^{-1} \tag{9}$$

Figure 4 shows a plot of the normalized intensity parameters for water droplets ($m = 1.33$) with a size parameter of 5. Note that the magnitude has been plotted in decibels. Most energy is scattered in the forward direction, but significant energy is scattered backwards and to the side with large variations as θ_s changes. Note that Rayleigh scattering is a limiting form of Mie scattering. In fact, Figure 3 was calculated and plotted using the Mie code, but with α set to 0.001.

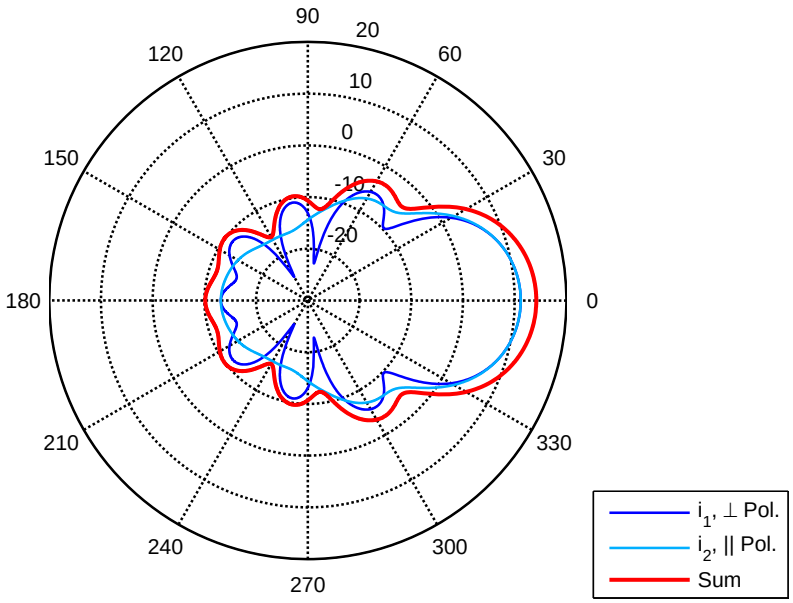

Figure 4: Mie phase function for $m = 1.33$ and $\alpha = 5$ in dB

To better verify the downloaded Mie code, a plot from [4] was regenerated. Figure 5 was generated using Mätzler's MATLAB Mie code. It matches the Figure 16.8 in Hinds [4].

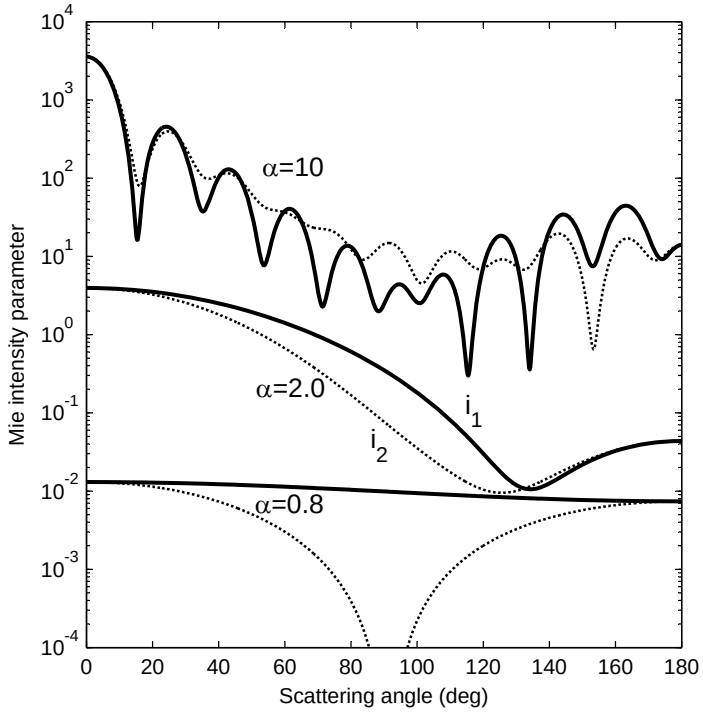

Figure 5: Mie intensity parameters for water droplets of various size parameters [4]

2 Diffuse UV Propagation

The propagation of UV light through the atmosphere over short distances can be described in terms of scattering and absorption. For molecular scattering, Rayleigh's theory can be used effectively. For particle diameters approaching the wavelength, however, scattering becomes much more complicated, and Mie scattering theory must be used [4].

An analytical non-line-of-sight (NLOS) single-scatter model for UV propagation has been published by Luettgen, Shapiro, and Reilly [7]. This model integrates scattered light from the intersection of two cones (representing the transmitter divergence and the receiver field-of-view) assuming that any light reaching the receiver sensor scattered only one time. This model is analytical, but the resulting equation requires numerical integration.

Luettgen's single-scatter model is somewhat of a standard in recent research—the results have been referenced by a number of other papers. However, some researchers have noted that the single-scatter model underestimates the delay spread and received power when compared to experimental measurements and Monte Carlo simulation[8, 9]. Still, the analytical model provides reasonable and convenient results.

We used Luettgen's model in our work to better understand system tradeoffs involved in designing a UV communication link. Luettgen's model assumes Rayleigh scattering. We modified the model to include the effect of Mie scattering in order to analyze the effects of obscurants such as fog and smoke. The following sections review Luettgen's model then describe the modifications introduced to incorporate Mie scattering.

2.1 Single Scatter Model

The model developed by Luettgen, Shapiro, and Reilly calculates the impulse response for optical radiation in a homogeneous scattering and absorbing medium [7]. Properties of the medium are incorporated using scattering and absorption coefficients. Setup of the calculation is straight-forward. However, calculating the intersection of two cones requires the use of a prolate-spheroidal coordinate system. The bulk of the paper deals with derivation of the integration limits. The setup and final results will be presented without showing the derivation. Interested readers should refer to the original results.

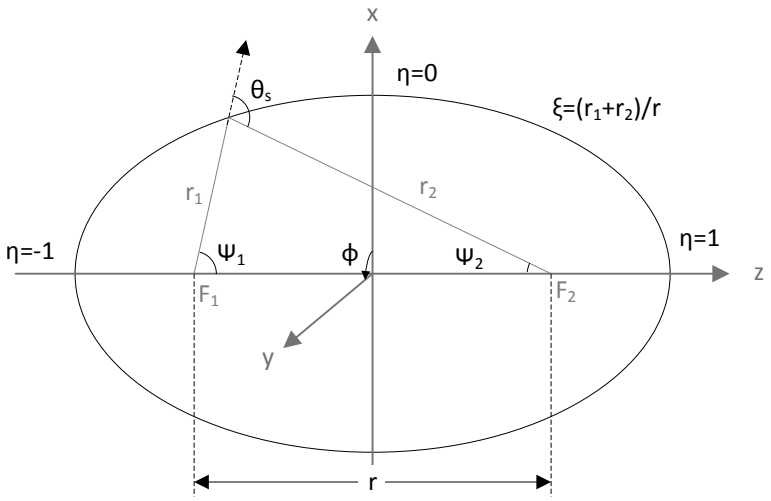

Figure 6: Prolate-spheroid coordinate system

The single-scatter model is based on the prolate-spheroidal coordinate system illustrated in Figure 6. This coordinate system is convenient because the sum of the distances from the focii to any point on the spheroid surface is constant (for a given ξ). In the single scatter model, this physically means that each value of ξ corresponds to a particular time delay in the impulse response. This relationship is given by Equation 10.

$$\xi = \frac{ct}{r} \tag{10}$$

Cartesian coordinates may be transformed into prolate-spheroidal coordinates by Equations 11 through 15.

$$\xi = (r_1 + r_2)/r \qquad (1 \leq \xi \leq \infty) \tag{11}$$

$$\eta = (r_1 - r_2)/r \qquad (-1 \leq \eta \leq 1) \tag{12}$$

$$\phi = \arctan(x, y) \qquad (-\pi \leq \phi \leq \pi) \tag{13}$$

$$r_1 = [x^2 + y^2 + (z + r/2)^2]^{1/2} \tag{14}$$

$$r_2 = [x^2 + y^2 + (z - r/2)^2]^{1/2} \tag{15}$$

The parameters ψ_1 and θ_s can be calculated as follows:

$$\cos\ \psi_1 = (1 + \xi\eta)/(\xi + \eta) \tag{16}$$
$$\sin\ \psi_1 = [(\xi^2 - 1)(1 - \eta^2)]^{1/2}/(\xi + \eta) \tag{17}$$
$$\cos\ \psi_2 = (1 - \xi\eta)/(\xi - \eta) \tag{18}$$
$$\sin\ \psi_2 = [(\xi^2 - 1)(1 - \eta^2)]^{1/2}/(\xi - \eta) \tag{19}$$
$$\cos\ \theta_s = (2 - \xi^2 - \eta^2)/(\xi^2 - \eta^2). \tag{20}$$

Figure 7 shows an example NLOS geometry with parameters labeled. The single-scatter model uses the following parameters:

θ_R Receiver half-field of view ($0 \leq \theta_R \leq \pi/2$) [rad]

β_R Receiver apex angle ($0 \leq \beta_R \leq \pi$) [rad]

θ_T Transmitter beam divergence half angle ($0 \leq \theta_T \leq \pi/2$) [rad]

β_T Transmitter apex angle ($0 \leq \beta_R \leq \pi$) [rad]

Q_T Energy of an impulse transmitted at time $t = 0$ [J]

k_s Atmospheric scatter coefficient [/m]

k_a Atmospheric absorption coefficient [/m]

k_e Atmospheric extinction coefficient [/m]

Ω_T Transmitter solid cone angle [sr]

$P(\theta_s)$ Normalized scattering phase function

$\mathbf{r}$ Interfocal distance [m]

The extinction coefficient is the sum of the scatter and absorption coefficients as shown in Equation 21.

$$k_e = k_s + k_a \tag{21}$$

When converting from beam divergence to solid angle, note that θ_T already represents the half-angle, as depicted in Figure 7. As a result, the solid angle is computer using Equation 22.

$$\Omega_T = 4\pi\ \sin^2(\theta_T) \tag{22}$$

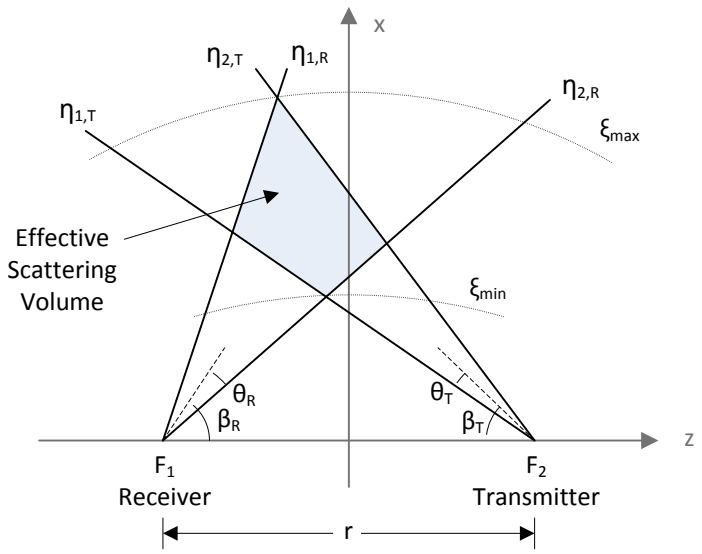

Figure 7: Non-line-of-sight geometry for single-scatter propagation model

To solve for the impulse response of the channel, first consider an impulse of energy Q_T emitted at time $t = 0$ from the transmitter. At a point P within the transmitter cone, the unextinguished energy per unit area at time $t = r_2/c$ is

$$H_P = \frac{Q_T \ \exp(-k_e r_2)}{\Omega_T (r_2)^2}. \tag{23}$$

The exponential term containing the extinction coefficient accounts for attenuation due to both scattering and absorption along r_2, the path from the transmitter to point P. The $(r_2)^2$ term in the denominator accounts for spreading losses. A differential volume δV enclosing P effectively becomes a new source, δQ_P.

$$\delta Q_P = k_s H_P \delta V \tag{24}$$

The energy emitted per unit solid angle from this source is

$$\begin{aligned}\delta R_P &= \delta Q_P \frac{P(\theta_s)}{4\pi} \\ &= k_s H_P \delta V \frac{P(\theta_s)}{4\pi} \\ &= \frac{k_s Q_T \ \exp(-k_e r_2)}{\Omega_T (r_2)^2} \delta V \cdot \frac{P(\theta_s)}{4\pi}. \end{aligned} \tag{25}$$

The volume element in prolate-spheroid coordinates is

$$\delta V = \frac{r^3}{8}(\xi^2 - \eta^2)\delta\xi\delta\eta\delta\phi. \tag{26}$$

Finally, the amount of scattered energy reaching the receiver is given in Equation 27. In this equation, ζ is the angle between the receiver axis and a vector pointing from the receiver and P.

$$\delta H_R = \delta R_P \frac{\cos(\zeta)\exp(-k_e r_1)}{(r_1)^2}. \tag{27}$$

Differential energy is converted to differential irradiance by substituting Equation 10, dividing by δt, and taking the limit as δt goes to zero.

$$\delta E(\xi) = \frac{Q_T c k_s \cos(\zeta)\exp(-k_e r\xi)}{2\pi\Omega_T r^2(\xi^2 - \eta^2)} P(\theta_s)\delta\phi\delta\eta \tag{28}$$

Integration over the surface of the prolate spheroid and then integrating again with respect to ϕ results in an equation for the impulse response of the channel. Equation 29 gives the result as irradiance (watts per square meter) as a function of time.

$$E(\xi) = \begin{cases} \dfrac{Q_t c k_s \exp(-k_e r\xi)}{2\pi\Omega_T r^2} \displaystyle\int_{\eta_1(\xi)}^{\eta_2(\xi)} \frac{2g[\phi_2(\xi,\eta)]P(\theta_s)}{\xi^2 - \eta^2}\,\mathrm{d}\eta, & (\xi_{min} \le \xi \le \xi_{max}) \\ 0, & \text{otherwise} \end{cases} \tag{29}$$

where

$$g[\phi_2(\xi,\eta)] = \phi_2(\xi,\eta)\cos(\beta_R)\cos(\psi_1) + \sin(\beta_R)\sin(\psi_1)\sin[\phi_2(\xi,\eta)]. \quad (30)$$

The values ξ_{min} and ξ_{max} are determined by the geometry of the transmitter and receiver. The two values correspond to the minimum and maximum time for which scattered energy is received for a transmitted impulse. They can be calculated using Equations 31 through 34.

$$\xi_{min} = \begin{cases} 1 & (\beta_r - \theta_r) \leq 0 \text{ or } (\beta_T - \theta_T) \leq 0 \\ a + (a^2-1)^{1/2} & 0 \leq (\beta_R - \theta_R) + (\beta_T - \theta_T) < \pi \\ \infty & \pi \leq (\beta_R - \theta_R) + (\beta_T - \theta_T) \end{cases} \quad (31)$$

$$\xi_{max} = \begin{cases} b + (b^2-1)^{1/2} & 0 \leq (\theta_R + \beta_R) + (\theta_T + \beta_T) < \pi \\ \infty & \pi \leq (\theta_R + \beta_R) + (\theta_T + \beta_T) \end{cases} \quad (32)$$

$$a = \frac{1 + \cos(\beta_R - \theta_R)\cos(\beta_T - \theta_T)}{\cos(\beta_R - \theta_R) + \cos(\beta_T - \theta_T)} \quad (33)$$

$$b = \frac{1 + \cos(\beta_R + \theta_R)\cos(\beta_T + \theta_T)}{\cos(\beta_R + \theta_R) + \cos(\beta_T + \theta_T)} \quad (34)$$

Deriving the limits of integration for Equation 29 is quite involved because of different tranmitter and receiver configurations which may or may not include the focii within the transmit and receive cones. The general solution is given by Equations 35 through 49.

$$\eta_1(\xi) = \max\{\eta_{1,R}, \eta_{1,T}\} \qquad (\xi_{min} \leq \xi \leq \xi_{max}) \quad (35)$$

$$\eta_2(\xi) = \min\{\eta_{2,R}, \eta_{2,T}\} \qquad (\xi_{min} \leq \xi \leq \xi_{max}) \quad (36)$$

$$\phi_2(\xi,\eta) = \min\{\phi_{2,R}(\xi,\eta), \phi_{2,T}(\xi,\eta)\} \qquad (\eta_1(\xi) \leq \eta \leq \eta_2(\xi)) \quad (37)$$

$$\eta_{1,R} = \begin{cases} -1 & (\beta_R + \theta_R \geq \pi) \\ \dfrac{\xi\cos(\beta_R + \theta_R) - 1}{\xi - \cos(\beta_R + \theta_R)} & (\beta_R + \theta_R \leq \pi) \end{cases} \tag{38}$$

$$\eta_{2,R} = \begin{cases} 1 & (\beta_R - \theta_R \leq 0) \\ \dfrac{\xi\cos(\beta_R - \theta_R) - 1}{\xi - \cos(\beta_R - \theta_R)} & (\beta_R - \theta_R \geq 0) \end{cases} \tag{39}$$

Note that the ranges for $\eta_{1,R}$ in Equation 38 were changed slightly from the paper to correct what I believe is a typo.

$$\phi_{2,R}(\xi,\eta) = \begin{cases} \pi & (\eta_{1,R} \leq \eta \leq \eta'_R \text{ and } \eta_{1,R} \neq \eta'_R) \\ f_R(\eta,\xi,\theta_R,\beta_R) & (\eta'_R \leq \eta \leq \eta''_R \text{ and } \eta'_R \neq \eta''_R) \\ \pi & (\eta''_R \leq \eta \leq \eta_{2,R} \text{ and } \eta''_R \neq \eta_{2,R}) \end{cases} \tag{40}$$

$$f_R(\eta,\xi,\theta_R,\beta_R) = \arccos\left(\frac{\cos\ \theta_R - \cos\ \beta_R\ \cos\ \psi_1}{\sin\ \beta_R\ \sin\ \psi_1}\right) \tag{41}$$

$$\eta'_R = \frac{\xi\cos(\theta_R + \beta_R) - 1}{\xi - \cos(\theta_R + \beta_R)} \tag{42}$$

$$\eta''_R = \frac{\xi\cos(\beta_R - \theta_R) - 1}{\xi - \cos(\beta_R - \theta_R)} \tag{43}$$

$$\eta_{1,T} = \begin{cases} -1 & (\beta_T - \theta_T \leq 0) \\ \dfrac{1 - \xi\cos(\beta_T - \theta_T)}{\xi - \cos(\beta_T - \theta_T)} & (\beta_T - \theta_T \geq 0) \end{cases} \tag{44}$$

$$\eta_{2,T} = \begin{cases} 1 & (\beta_T + \theta_T \geq \pi) \\ \dfrac{1 - \xi\cos(\beta_T + \theta_T)}{\xi - \cos(\beta_T + \theta_T)} & (\beta_T + \theta_T \leq \pi) \end{cases} \tag{45}$$

The denominator for the second case of Equation 45 has been changed from $\xi - \cos(\theta_T - \beta_T)$. This is probably another small typo in the paper.

$$\phi_{2,T}(\xi,\eta) = \begin{cases} \pi & (\eta_{1,T} \leq \eta \leq \eta'_T \text{ and } \eta_{1,T} \neq \eta'_T) \\ f_T(\eta,\xi,\theta_T,\beta_T) & (\eta'_T \leq \eta \leq \eta''_T \text{ and } \eta'_T \neq \eta''_T) \\ \pi & (\eta''_T \leq \eta \leq \eta_{2,T} \text{ and } \eta''_T \neq \eta_{2,T}) \end{cases} \tag{46}$$

$$f_T(\eta, \xi, \theta_T, \beta_T) = \arccos\left(\frac{\cos\ \theta_T - \cos\ \beta_T\ \cos\ \psi_2}{\sin\ \beta_T\ \sin\ \psi_2}\right) \tag{47}$$

$$\eta'_T = \frac{1 - \xi\cos(\beta_T - \theta_T)}{\xi - \cos(\beta_T - \theta_T)} \tag{48}$$

$$\eta''_T = \frac{1 - \xi\cos(\beta_T + \theta_T)}{\xi - \cos(\beta_T + \theta_T)} \tag{49}$$

The equations presented up to this point are used to calculate the impulse response of the channel. From the impulse response, the total energy density at the receiver (in joules per square meter) can be calculated as shown in Equation 50.

$$H_R = \int_{t_m in}^{tmax} E(ct/r)\ \mathrm{d}t \tag{50}$$

These equations were programmed into MATLAB. Numerical integration of Equation 29 was performed using MATLAB's built-in adaptive Gauss-Kronrod quadrature algorithm, `quadgk`. To check the functionality of the code, an example result in the paper was regenerated. Figure 8 shows a comparison of the impulse response calculated using our MATLAB code. The results match—with one small caveat.

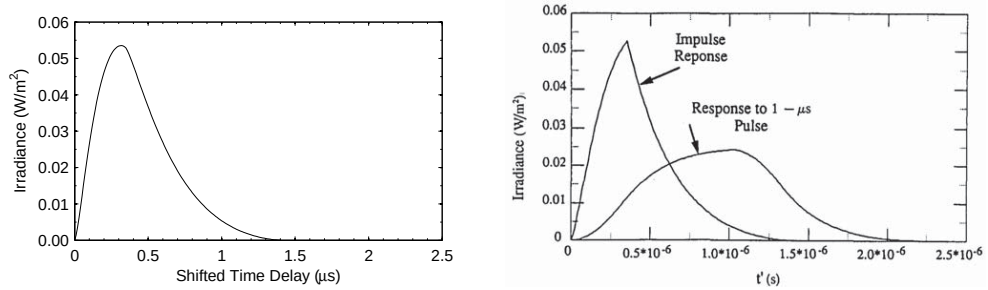

(a) MATLAB results

(b) Published results from [7], Figure 10

Figure 8: Comparison with published results

The parameters used to obtain this result were as follows: $r = 500\,\mathrm{m}$, $\theta_T = \theta_R = \pi/12$, $\beta_R = \beta_T = \pi/4$, $Q_T = 1\,\mathrm{J}$. A wavelength of 250 nm was

assumed, and some reasonable values for the atmospheric coefficients were chosen: $k_a = k_s = 5 \times 10^{-4}$. The phase function, $P(\theta_s)$, was set to 1. In addition, the paper converts from transmitter divergence to solid angle by using $Q_T = 4\pi \sin^2(\theta_T/2)$. However, since θ_T is already the half-angle, it should not be divided by two. In order to make the results match, a divide by two was introduced into the code for this plot only.

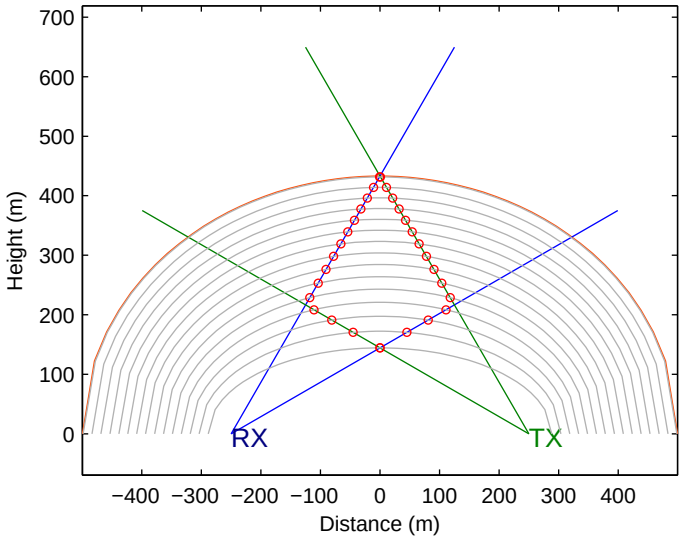

Figure 9: Receiver and transmitter geometry for example results

Figure 9 plots the transmit/receive cones as well as the elliptical contours at 0.1 µs spacing. For each value of ξ, Equation 29 is integrated along the gray contour between the limits $\eta_1(\xi)$ and $\eta_2(\xi)$, which are marked by red circles.

2.2 Modified Scatter Model

The material presented in the previous section was taken directly from Luettgen's paper. In order to model the effects of obscurants such as fog and smoke, Mie scattering must be taken into account because the aerosol particle diameters are comparable to mid-UV wavelengths. The Rayleigh scattering approximation only holds when particle diameters are much smaller than the wavelength [4].

Under the single-scatter assumption, effects from the scattering and absorption caused by obscurants can simply be added to the scattering and absorption due to molecular scattering characterized by Rayleigh's equations. Obscurant particles add both additional attenuation as well as additional scattering.

To accommodate the possibility of mixed obscurants with different density, particle diameters, and composition, we introduce a discretized population of particle diameters, D_i. For each value of D, there is an associated concentration, C_i, and an associated complex refractive index, M_i. From these, we calculate extinction, scattering and absorption coefficients ($k_e m, i$, $k_s m, i$ and $k_a m, i$) using the Mie code for each index i. The subscript m has been appended to distinguish the new Mie coefficients from the Rayleigh coefficients. The particle size distribution is discrete for simplicity, but the number of bins can be made arbitrarily small if greater resolution is required.

The equations from Luettgen's paper can now be modified to accomodate the added particulates. Starting with Equation 23, additional attenuation is included to account for added particles in the propagation path. The modified equation, Equation 51, shows the unextinguished energy per unit area at the scattering point, P, after adding this attenuation. Modified equations are marked with a $'$ symbol.

$$\begin{aligned} H'_P &= \frac{Q_T}{\Omega_T (r_2)^2} \left[\mathrm{e}^{-k_e r_2} \mathrm{e}^{-k_{em,1} r_2} \mathrm{e}^{-k_{em,2} r_2} \dots \right] \\ &= \frac{Q_T}{\Omega_T (r_2)^2} e^{-K_e r_2} \end{aligned} \tag{51}$$

In the second line, the Rayleigh and Mie coefficients have been combined into a total extinction coefficient, K_e.

$$K_e = k_e + \sum_i k_{em,i} \tag{52}$$

Continuing with the modification, the energy scattered from location P is

$$\delta Q'_P = k_s H'_P \delta V + \sum_i k_{sm,i} H'_P \delta V. \tag{53}$$

Applying the Rayleigh phase function, $P_r(\theta_s)$, and Mie phase functions, $P_{m,i}(\theta_s)$, to the appropriate terms, the energy transmitted from P per unit solid angle is then

$$\delta R'_P = \left[k_s H'_P \frac{P_r(\theta_s)}{4\pi} + \sum_i k_{sm,i} H'_P \frac{P_{m,i}(\theta_s)}{4\pi} \right] \delta V. \tag{54}$$

Note that for each particle index, i, there is a different scattering coefficient, $k_{sm,i}$, and phase function, $P_{m,i}(\theta_s)$. The energy from all these contributions are summed for a particular scattering angle, θ_s.

At the receiver, the energy per unit area in prolate-spheroid coordinates is

$$\delta H'_R = \delta R'_P \frac{\cos(\zeta) \exp(-K_e r_1)}{(r_1)^2}. \tag{55}$$

In comparison to Equation 27, δR_P has been replaced with $\delta R'_P$ and k_e has been replaced with K_e. Following the same manipulations as for Equation 28, we obtain the irradiance at the receiver sourced by a differential volume on the spheroid specified by ξ, $E'(\xi)$.

$$\begin{aligned} \delta E'(\xi) = & \frac{Q_T c k_s \cos(\zeta) \exp(-K_e r \xi)}{2\pi \Omega_T r^2 (\xi^2 - \eta^2)} P_r(\theta_s)\, \delta\phi \delta\eta + \\ & \sum_i \frac{Q_T c k_{sm,i} \cos(\zeta) \exp(-K_e r \xi)}{2\pi \Omega_T r^2 (\xi^2 - \eta^2)} P_{m,i}(\theta_s)\, \delta\phi \delta\eta \end{aligned} \tag{56}$$

Integrating as before and switching the order of summation and integration gives the received irradiance, $E'(\xi)$, for values of ξ between ξ_{min} and ξ_{max}. ($E'(\xi)$ is zero outside this range.) The limits of integration remain unchanged from the original model.

$$\begin{aligned} E'(\xi) = & \frac{Q_t c k_s \exp(-K_e r \xi)}{2\pi \Omega_T r^2} \int_{\eta_1(\xi)}^{\eta_2(\xi)} \frac{2g[\phi_2(\xi,\eta)] P_r(\theta_s)}{\xi^2 - \eta^2}\, \mathrm{d}\eta + \\ & \sum_i \left[\frac{Q_t c k_{sm,i} \exp(-K_e r \xi)}{2\pi \Omega_T r^2} \int_{\eta_1(\xi)}^{\eta_2(\xi)} \frac{2g[\phi_2(\xi,\eta)] P_{m,i}(\theta_s)}{\xi^2 - \eta^2}\, \mathrm{d}\eta \right] \end{aligned} \tag{57}$$

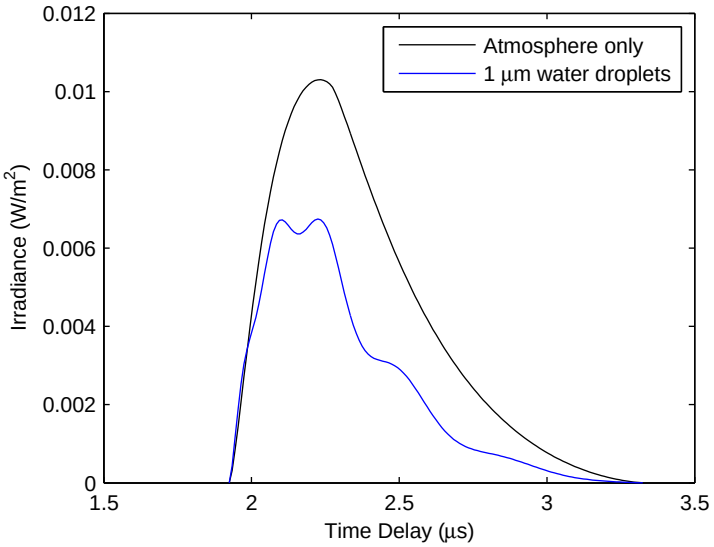

Figure 10: Example output comparing clear atmosphere versus fog

Comparing with Equation 29, we see that the scattering contribution from each particle type (each index, i) is added after integration over the prolate spheroid. The phase function must be calculated for each particle type. Attenuation caused by particulates are included in the total extinction coefficient, K_e, which is simply the sum of all the individual extinction coefficients. Note that the extinction coefficients are specific to a particular concentration, particle diameter, and composition.

From a programming point of view, the modification to the MATLAB code that implements Luettgen's model is straight-forward. Given the array of particles sizes and their characteristics, coefficients are calculated using the Mie code. The total extinction coefficient is computed by summing all the extinction coefficients. The irradiance is then computed for each particle type separately (the phase function is specified uniquely by the particle size parameter and the index of refraction), and the result is summed.

Figure 10 shows example results comparing the impulse response for clear atmosphere versus a monodisperse fog of 10^9particles/m^3, 1 µm water droplets given the same geometry as shown in Figure 9 and 1 J of transmitted energy at 250 nm.

With a wavelength of 250 nm, the size parameter, α, is 12.6. The phase

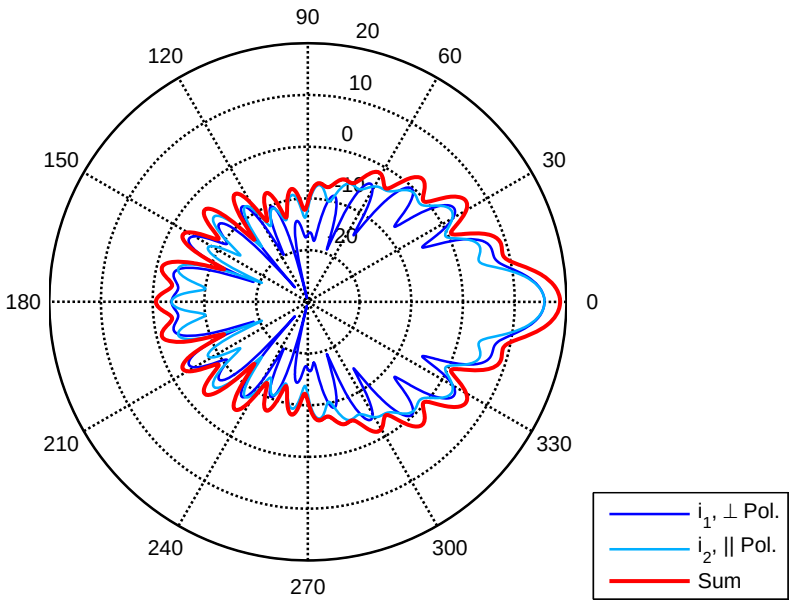

Figure 11: Phase function for $m = 1.33$ and $\alpha = 12.6$ in dB

function for such a relatively large particle is shown in Figure 11, plotted in dB.

This example includes only a single particle type, but the computer code allows the addition of an arbitrary distribution of particles.

3 Analysis

This section uses the computer model to analyze a system varying the following parameters:

1. wavelength
2. obscurants (representative fog, smoke, clear)
3. transmitter power, divergence angle, elevation angle
4. receiver field of view, elevation angle
5. tx/rx separation
6. filter parameters

Parameters should be defined based on available components (or components in development)

The outputs to be compared are:

1. energy density
2. delay spread
3. peak irradiance
4. E_b/N_0, bit error rate

References

[1] Gary A. Shaw et al. Recent progress in short-range ultraviolet communication. *SPIE*, 5796:214–225, 2005.

[2] Zhengyuan Xu and Brian M. Sadler. Ultraviolet communications: Potential and state-of-the-art. *IEEE Communications Magazine*, 2008.

[3] David M. Reilly et al. Unique properties of solar blind ultraviolet communication systems for unattended ground sensor networks. *SPIE*, 5611:244–254, 2005.

[4] William C. Hinds. *Aerosol Technology*. John Wiley and Sons, 2nd edition edition, 1999.

[5] Ronald C. Taylor et al., editors. *AMS Glossary of Meteorology*. `http://amsglossary.allenpress.com/glossary`, 2nd edition.

[6] Christian Matzler. Matlab functions for mie scattering and absorption. Research Report 2002-08, Institut fur Angewandte Physik, 2002. Report: `http://arrc.ou.edu/~rockee/NRA_2007_website/Mie-scattering-Matlab.pdf`, Code: `http://diogenes.iwt.uni-bremen.de/vt/laser/codes/Mie-Matlab-Maetzler.zip`.

[7] Mark R. Luettgen et al. Non-line-of-sight single-scatter propagation model. *Journal of the Optical Societ of America*, pages 1964–1972, 1991.

[8] Haipeng Ding et al. Modeling of non-line-of-sight ultraviolet scattering channels for communication. *IEEE Journal on Selected Areas in Communication*, 2009.

[9] Zhengyuan Xu et al. Analytical performance study of solar blind non-line-of-sight ultraviolet short-range communication links. *Optics Letters*, pages 1860–1862, 2008.